Exp Fluids (2008) 45:999–1013
DOI 10.1007/s00348-008-0522-4

RESEARCH ARTICLE

Quantitative characterization of coherent structures in the buffer layer of near-wall turbulence. Part 1: streaks

J. Lin · J. P. Laval · J. M. Foucaut · M. Stanislas

Received: 26 November 2007 / Revised: 25 April 2008 / Accepted: 16 May 2008 / Published online: 17 June 2008

Abstract Streaks play a major role in the process of turbulent generation. Numerous studies have been performed to characterize them, most of which used only single point measurements and only a few characteristics were studied. To investigate the streaks in more detail, a stereoscopic particle image velocimetry (SPIV) experiment was conducted to record 2D3C velocity fields in ten planes parallel to the wall from $y^+ = 14.5$ to $y^+ = 48$ at Reynolds number $Re_\theta = 7{,}800$ in a fully developed turbulent boundary layer along a flat plate. This study develops a method based on pattern recognition to detect streaks from velocity fields obtained by SPIV and characteristizes them in depth. The results are in good agreement with the previous studies and expand significantly the information about the characteristics of the streaks.

1 Introduction

Streaks, which are elongated regions of slow or fast fluid (compared to the mean), more or less aligned in the streamwise direction, are important phenomenon occuring in the viscous and buffer layers of near-wall turbulence. They were first identified by Hama (1954) in his flow visualization experiments. He observed that very near to the wall, the instantaneous spanwise distribution of streamwise velocity consists of alternating regions of high- and low-speed fluids. Since then, streaks have been identified and examined by a number of authors under different experimental conditions.

J. Lin · J. P. Laval · J. M. Foucaut · M. Stanislas (✉)
Laboratoire de Mechanique de Lille (LML), Bd. Paul Langevin, Cite Scientifique, Lille 59655, France
e-mail: michel.stanislas@ec-lille.fr

Kline et al. (1967) investigated boundary layers subject to different pressure gradients by using hydrogen bubble wire visualization technique. They observed that low-speed streaks exist in all cases, including those in which relaminarization can occur. Even after being disrupted, streaks can quickly re-establish. Additionally, streaks show a remarkable degree of persistence and regularity. Bippes (1972) investigated a transitional boundary layer on a concave surface and observed these streaky structures by using the same hydrogen bubble wire visualization technique as used by Kline et al. (1967). The visualization picture he obtained is extraordinarily similar to those obtained by Kline et al. (1967) in a fully turbulent boundary layer. Therefore, Kline (1978) suggested that streaks constitute a universal feature of bounded shear flows and that the presence of streaks is a sufficient condition for establishing whether a given boundary layer flow is turbulent.

Thereafter, many properties of streaks have been investigated. These structures are most clearly observed very close to the wall. Moving away from it, fewer and fewer streaks are found. Low-speed streaks are not rigidly directed along the streamwise direction but show time-dependent meanders in the spanwise direction where they merge together or separate (Talmon et al. 1986; Johansson et al. 1991; Landahl 1990). Compared to low-speed streaks, high-speed streaks were less investigated. Talmon et al. (1986) found that high-speed streaks are related to regions of high value of the Reynolds stresses. The studies of Suzuki and Kasagi (1993) and Robinson (1991) associated high-speed streaks with an exchange between wall-normal velocity and streamwise or spanwise velocity. Johansson et al. (1991) observed that the high-speed streaks are surrounded by spanwise diverging fluid.

Many efforts have been made to quantify the physical characteristics of streaks. Most of studies focused on the

mean spanwise spacing. Runstadler et al. (1963) were the first to carry out a systematic and quantitative investigation of streaks, which showed that the mean spacing between streaks could be quantified and correlated. Schraub and Kline (1965) established the mean spanwise spacing between low-speed streaks by using primarily flow visualization techniques for low Reynolds number flows ($Re_\theta < 1{,}500$). They found that the mean spanwise spacing is generally about 100 ± 20 wall units. Many researchers (e.g., Oldaker and Tiederman 1977; Achia and Thompson 1977; Lee et al. 1974; Blackwelder and Eckelmann 1979; Kreplin and Eckelmann 1979) have confirmed this value with different visual and probe experiment techniques. Using flow visualization experiment at $740 < Re_\theta < 5{,}380$, Smith and Metzler (1983) found that the mean spanwise spacing of low-speed streaks is about 100^+ based on a detection threshold. For a higher Reynolds number ($Re_\theta > 4{,}700$), Gupta et al. (1971) investigated the spatial structure in the viscous sublayer using an array of hot-wires distributed in the spanwise direction. They used a VITA correlation technique to determine the spanwise separation between streaks in the viscous sublayer. Their results show that the mean spacing increases with Reynolds number (up to 10,000), which reveals a dependence of this spacing on Reynolds number. This conclusion is also confirmed by recent research (Kaehler 2004; Lagraa et al. 2004; Carlier and Stanislas 2005). In case of low Reynolds numbers, the nondimensional mean streak spacing was suggested to be invariant (Kline et al. 1967; Achia and Thompson 1977; Oldaker and Tiederman 1977; Nakagawa and Nezu 1981; Smith and Metzler 1983). This value is generally accepted as 100 ± 20 wall units for $y^+ \leq 10$ and increases for $y^+ > 10$.

Besides the mean spanwise spacing, the mean length and width of streaks were also investigated. Blackwelder and Eckelmann (1979) used a combination of hot film probes and flush mounted surface elements to measure the length of streaks in a low Reynolds number oil channel. They found that streamwise length scales can extend beyond $\Delta x^+ > 1{,}000$ according to the connected regions of low axial velocity in the region $5 \leq y^+ \leq 30$. Oldaker and Tiederman (1977) also found that streaks may exceed $\Delta x^+ > 1{,}000$ by their dye visualization experiment. Kreplin and Eckelmann (1979), using the same oil-channel facility as used by Blackwelder and Eckelmann (1979), confirmed these results by their probe correlation studies. By using a stereoscopic particle image velocimetry (SPIV) experiment, Carlier and Stanislas (2005) confirmed this result by their own experiments and agreed that the streamwise size of streaks is generally between 500 and 2000 wall units. Moreover, they also found that the width of streak is between 20 and 40 wall units.

Particle image velocimetry (PIV) (Adrian 1991) can measure two velocity components in a plane of observation. However, it is sometimes rather difficult to understand the true physical significance of the observed flow phenomena without the third component. This is particularly true in turbulence. To solve this problem, the method of Stereoscopic PIV was introduced by Prasad and Adrian (1993) to obtain the three-dimensional velocity field in a plane. In this method, a stereoscopic camera system is introduced, in which the motion of the tracer particles is viewed from two different directions. From the differences in the apparent in-plane motion obtained by each camera, it is possible to reconstruct all three components of the displacement and thus to obtain instantaneous 2D3C velocity fields. In the past decade, this method has been well developed and applied by a number of researchers (Soloff et al. 1997; Willert 1997; Westerweel and van Oord 1999; Coudert and Schon 2001). The SPIV method can now reach an accuracy as good as standard PIV (Pérenne et al. 2004).

The main objectives of the present study are to identify streaks from a database that was obtained in the near-wall region of a turbulent boundary layer ($14.5 < y^+ < 48$) by a SPIV experiment and to investigate the characteristics of these streaks (such as size, periodic spacing, etc.). This paper proceeds as follows. Section 2 introduces the SPIV experimental setup. Section 3 describes the procedure for detecting streaks. Section 4 presents and discusses the results, followed by conclusions in Section 5.

2 Experiment

The purpose of the experiment was to obtain 3C velocity fields in planes parallel to the wall of a boundary layer, as close as possible to the wall. The experiment was carried out in a boundary layer wind tunnel (Carlier 2001), which is 1×2 m^2 in cross section and 21.6 m in length. A Nd-YAG pulsed laser, with 2×250 mJ of energy at 15 Hz, was used to generate the light sheet. This light sheet was shaped using a conventional optical set-up (one spherical and one cylindrical lens) with a thickness of about 0.75 mm. The light sheet passed through a lateral window located 1 m away from the measurement area. Two PCO SENSICAM cameras ($1{,}280 \times 1{,}024$ Pixel^2) were positioned under the wind tunnel as shown in Fig. 1. The cameras were set in the Scheimpflug conditions (Willert 1997). The H and L parameters defined in Fig. 1 are as follows: $H \cong 52$ cm and $L \cong 50$ cm. These distances, which are necessary for the geometrical reconstruction, are measured with respect to the centre of the field of view. The line joining the two cameras is parallel to the main flow (camera #1 being upstream). The flow is from left to right in the images delivered by both cameras. The light sheet propagates in the test section along z. Both cameras stand on the same ground

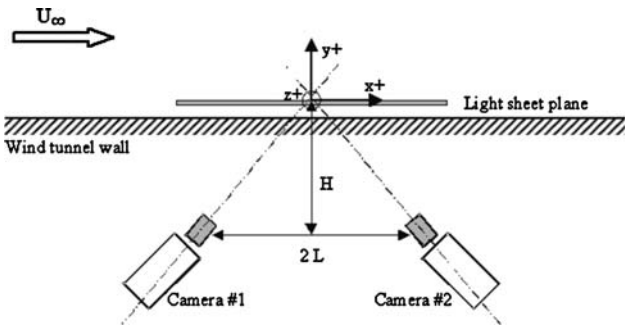

Fig. 1 Setup of the experiment and frame of reference for data analysis

under the wind tunnel upstream and downstream of the light sheet to obtain symmetric light-scattering conditions. The focal length of the camera lenses was 105 mm. The field of view extends over 6.5 × 4.0 cm^2 and an f-stop of $f_{\#} = 5.6$ was used for both cameras during the experiments. The average magnification was approximately 50 μm/pixel in the object space. The depth of field was 3.5 mm. The focus was set at the middle value of the explored y domain and kept there for the remainder of the experiment (including the acquisition of calibration images). The experiments were performed at $U = 3$ m/s (free stream velocity). With this velocity, the Reynolds number Re_θ, based on the momentum thickness, is 7,800. The friction velocity u_τ is of the order of 0.15 m/s. A wall unit ($\Delta y^+ = 1$) is 0.125 mm. Ten planes parallel to the wall were characterized. A total of 500 image pairs in each plane were recorded for each camera. The first plane was placed as near as possible to the wall while avoiding too much reflections. The spacing between two neighboring planes was about 4 wall units. This flow presents a tiny longitudinal pressure gradient, which is negligible and has no effect on the near-wall turbulence. The instantaneous velocity fields were calculated using the Soloff method (Soloff et al. 1997) and were validated by an earlier study (Lin et al. 2008).

3 Detection of streaks

In the present study, a method based on pattern recognition is developed to identify and characterize both low- and high-speed streaks from the instantaneous velocity fields provided by SPIV.

It is performed in four steps:

1. Detection function definition: to define the detection function according to the property of structures.
2. Thresholding: to generate binary indicative images.
3. Mathematical morphology: to remove noise and improve the quality of each binary image.
4. Cleaning: to remove the spurious objects.

3.1 Detection function definition

To identify the structure objects, a detection function or a group of detection functions, which describe(s) their basic characteristic(s), has to be defined. The function is generated according to the property of the structures, which are inferred from the observations in the experiments or numerical simulations. It is well known that low- and high-speed streaks correspond to low and high streamwise velocity (u component) distribution relative to the mean $\bar{u}$, in other words, high-velocity fluctuations of the streamwise component. According to this definition, different methods have been proposed to identify low-speed streaks. Gupta et al. (1971) have used a VITA method in their investigations using hot wires. Smith and Metzler (1983) have performed an experiment with a high-speed video system and hydrogen bubble-wire flow visualization. They identified low-speed streaks by considering the differential in momentum flux between the adjacent high- and low-speed regions. By applying the autocorrelation method to the streamwise velocity fluctuation u', Kaehler (2004) has evidenced the existence of streaks. However, most of these detections were specified to calculate one or several spatial characteristics (mainly frequency of appearance and spanwise spacing). Benefiting from instantaneous velocity fields obtained from PIV experiments, Carlier and Stanislas (2005) are one of the early researchers who have made efforts to obtain the instantaneous streak images. They applied a threshold directly to the normalized streamwise velocity fluctuation field to generate the instantaneous binary image of streaks. All abovementioned methods are based on the streamwise velocity or its fluctuations. As both of them are widely agreed to be the characteristic variables of streaks, it is reasonable to choose one or the other as the detection variable. In the present study, the velocity fluctuations are normalized with the standard deviation. The detection function (F_d) of streaks is defined as

$$F_\mathrm{d} = f(u'(m,n,y^+), \sigma_u(y^+)) = \frac{u'(m,n,y^+)}{\sigma_u(y^+)} \quad (1)$$

where u' is the instantaneous velocity fluctuation of the streamwise component u, σ_u is the standard deviation, (m, n) is the position in the (M, N) grid (velocity field obtained from SPIV database), and y^+ is the wall distance at which the SPIV measurement is performed.

3.2 Thresholding

In the present study, the detection function F_d given in Eq. 1, is a real scalar field defined on a discrete (M, N) grid in R^2. Streaks are detected by applying a threshold C_T directly to F_d. The value of C_T is taken positive. The

corresponding binary image is called indicative function F_i, which is defined as

$$\text{Low-speed streaks } F_i = \begin{cases} 1 & \text{when } F_d < -C_T \\ 0 & \text{otherwise} \end{cases} \quad (2)$$

$$\text{High-speed streaks } F_i = \begin{cases} 1 & \text{when } F_d > C_T \\ 0 & \text{otherwise} \end{cases} \quad (3)$$

In the present study, C_T was selected as 0.6 at $y^+ = 14.5$. As is well known, $\sigma^n{}_u$ decreases with wall distance when $y^+ > 10-15$. Also, beyond a certain distance from the wall, streaks are known to disappear. Considering these facts, the threshold C_T for the other wall distances was chosen as $0.6 \times \sigma_u^{\max}/\sigma_u^n$. Here, σ_u^n is the standard deviation of the streamwise velocity component u at position n, and $\sigma_u^{\max}$ is the maximum standard deviation of the present flow and is equal to 0.35 according to our previous study (Lin et al. 2008). According to this method, there is a streak only when u' (fluctuation of the streamwise velocity) is larger than a constant value whatever the wall distance is. Table 1 gives the resulting values of C_T at each wall distance studied.

3.3 Mathematical morphology

Because of the measurement noise, the indicative function F_i obtained directly from the thresholding procedure is relatively noisy. To improve it, a mathematical morphology procedure is employed. Mathematical morphology is a methodology for image analysis, which aims at quantitatively describing the geometrical structure of image objects. The basic morphological transformations that can be applied to a discrete binary set A are dilation and erosion, which are based on Minkowski algebra (Matheron 1975). Let B be also a set of the same commutative group. The dilation of A by B, noted $\delta_B(A)$, is the Minkowski addition $(\oplus)$ of A and B, while the erosion, noted $\varepsilon_B(A)$, is the Minkowski subtraction $(\ominus)$ of B from A. They are defined by

$$\begin{aligned} \delta_B(A) &= A \oplus B = \bigcup(\{x\} + B; \{x\} \in A) \\ \varepsilon_B(A) &= A \ominus B = \bigcup(\{x\}; \{x + B\} \in A) \end{aligned} \quad (4)$$

In practice, the set A will be the indicative function F_i created by the filtering or thresholding procedure, which has values 1 for the image objects and 0 for the background. The set B will be referred to as a structuring element. For a binary set, the structuring element contains two values: 1 and 0. It can be defined as any shape according to the application. Single dilation or erosion expands or reduces the image objects and thus results in the global geometric distortion of unsuppressed features. To avoid this effect, dilation and erosion are often combined in pairs to be used, in either of two ways, to produce fundamental morphological operations called closing and opening. Opening is simply an erosion followed by a dilation and closing is the opposite. Opening breaks narrow isthmuses, eliminate small islands and sharp peaks or capes. Closing fuses narrow breaks and long thin gulfs, and fills in the thin gulfs and small holes.

To improve the present binary image (indicative function F_i), a closing operation is used firstly to connect separated objects and to fill in holes by changing the value of F_i from 0 to 1 in the corresponding position. Then an opening operation is employed to remove isolated small objects, sharp peaks or capes by changing the value of F_i from 1 to 0 in the corresponding position. As mentioned above, a structuring element needs to be defined before processing those operations. In the present study, the structuring element is referred to as parameter M_S and is chosen according to the shape of objects expected. Since streaks are elongated in the streamwise direction, a rectangular structuring element was chosen: $M_S(W, L)$, in which W is the width in the spanwise direction and L is the length in the streamwise direction. The values of W and L are given in wall units. After a detailed study (Lin 2006), the structuring element was selected as $M_S = (10^+, 50^+)$ for both low- and high-speed streaks in the present study.

3.4 Cleaning procedure

After the mathematical morphology procedure, many small objects, whose surfaces are larger than that of the structuring element but not enough to be considered as expected coherent structures (streaks in the present study), remain in the images. They should be removed before statistical analysis. Therefore, a cleaning procedure with two parameters is introduced to remove these objects by considering their areas. One is for the objects that are cut by

Table 1 Threshold C_T in ten planes of measurement ($\sigma_u^{\max} = 0.35$)

	Plane #									
	1	2	3	4	5	6	7	8	9	10
y^+	14.5	18.5	22.2	26.3	29.7	33.3	37.0	40.6	44.0	48.0
σ_u^n	0.348	0.344	0.329	0.322	0.316	0.307	0.298	0.293	0.288	0.281
$C_T = 0.6 \times \sigma_u^{\max}/\sigma_u^n$	0.60	0.61	0.63	0.65	0.66	0.68	0.70	0.72	0.72	0.74

borders and the other is for the small objects totally embedded in the images. They are named 'clean factor for incomplete objects cut by borders' (referred to as C_B) and 'clean factor for complete objects' (referred to as C_C), respectively. Let us take A_s as the object area. The cleaning procedure is defined as

$$\text{For a complete object } F_i = \begin{cases} 0 & \text{when } A_s \le C_C \\ 1 & \text{otherwise} \end{cases} \quad (5)$$

$$\text{For an incomplete object } F_i = \begin{cases} 0 & \text{when } A_s \le C_B \\ 1 & \text{otherwise} \end{cases} \quad (6)$$

The two clean factors C_B and C_C are given in square wall units. The values $C_B = 1{,}750^{+2}$ and $C_C = 2{,}500^{+2}$ were chosen for both low- and high-speed streaks. It should be noted that the value of C_B is larger than half of the value of C_C due to the fact that streaks are much larger than the average size of complete objects obtained in the present study. Figure 2 shows an example of detection function and the corresponding indicative image of streaks at different steps of the detection procedure. In this figure, the structures and the background are represented respectively by white and black in all binary images. Details about the selection of these parameters are described by Lin (2006).

Ganapathisubramani et al. (2003) were among the first who made efforts to obtain the instantaneous streak images. They developed an objective feature extraction algorithm to detect different coherent structures including streaks. However, as noted by themselves, they detected some individual short patches, which were supposed to be part of long ones, but their technique could not reconnect them. This problem was solved in the present method by introducing a mathematical morphology procedure. Moreover, an additional cleaning procedure in the present method has been used to remove spurious objects, and thus to improve the accuracy of the statistical results.

3.5 Various conditions and interesting characteristics

As the velocity fields are in a limited area, the streaks may have various locations. Taking this into account, four circumstances are considered when statistical results are computed. This is illustrated in Fig. 3, where 0 and 1 indicate background (white) and objects (gray), respectively. In the first case (Fig. 3a), streaks are embedded totally in the image area without holes inside or branches. The principal statistical characteristics that can be computed are frequency of appearance (N_f) (number of objects per image), spanwise angle (φ), width (W), length (L), spanwise distance (d) between two nearby objects, streamwise distance (d_s) and area (A_c). In the present study, spanwise distance between two closest objects can be also obtained and it is named (d_n). For example, in

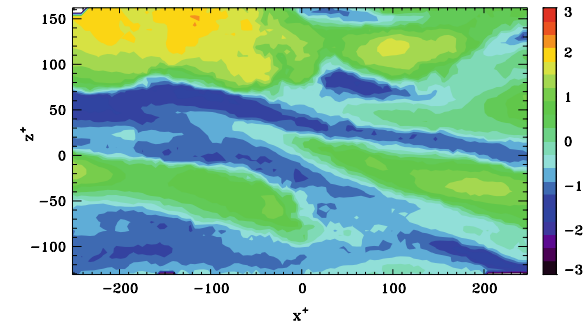

Detection function


After thresholding


After mathematical morphology


After cleaning

Fig. 2 Detection image and indicative images

Fig. 3a, there are three objects. Taking the object at the bottom as a reference, the middle object can be referred to as a closest object while the upper one as a nearby object. The spanwise distance between the bottom object

and its closest neighbor is named not only d but also d_n. Clearly, d includes all d_n. It should be noted that the streamwise size of the velocity field is about 530 wall units. As is well known, the length of streaks is generally between 500 and 2,000 wall units. Thus, for streaks, it is not possible to obtain the information about length (L), area (A_c), and streamwise distance d_s in the present study.

In the second case (Fig. 3b), objects are cut by the spanwise borders. Only the number of object (N_f) can be obtained. The other parameters cannot be calculated, since there is no information on the portion of objects beyond the image.

In the third and fourth cases (Fig. 3c, d), objects have more than one branch or have large holes inside them. The distance between objects can be determined similarly as in case one. Given that the images are M lines in the streamwise direction x and N columns in the spanwise direction z, the width can, however, be calculated as $W^j = (\sum_{i=1}^{b} W_i)/b$. Here, j is the index of the column, b is the number of branches, and W_i is the width of each branch. The distance and the width are measured in the spanwise direction z for each column. The mean distance $\bar{d}$ is taken as the average of all measurements. The width of each object $\bar{W}$ is calculated by averaging W^j. These, of course, can be averaged again over all the objects, yielding mean width $\overline{W_a}$.

4 Results and discussions

4.1 Frequency of appearance

One interesting characteristic of streaks is the frequency of appearance, in other words, the number of streaks in a certain area. In the present study, the area (field of view) is $530^+ \times 300^+$ in a streamwise–spanwise plane. Figure 4 shows frequency of appearance of detected streaks (N_f) based on this area at various wall distances. Low- and high-speed streaks are represented by LSS and HSS, respectively, in all the figures if no other specification is made. In Fig. 4, the error bars represent an error of 5% of the mean. In the lower part of the buffer layer ($y^+ \leq 30$), low- and high-speed streaks show a different behavior. As wall distance increases, the frequency N_f decreases relatively rapidly for high-speed streaks but is nearly the same or decreases very slowly for low-speed ones. In the upper part of the buffer layer ($y^+ > 30$), the frequency of both types of streaks show the same decreasing rate with wall distance. On average, about 2.9 low-speed streaks and 2.8 high-speed ones are expected per area of $530^+ \times 300^+$ at $y^+ = 14.5$, while about 2.1 low-speed and 1.6 high-speed streaks at $y^+ = 48$.

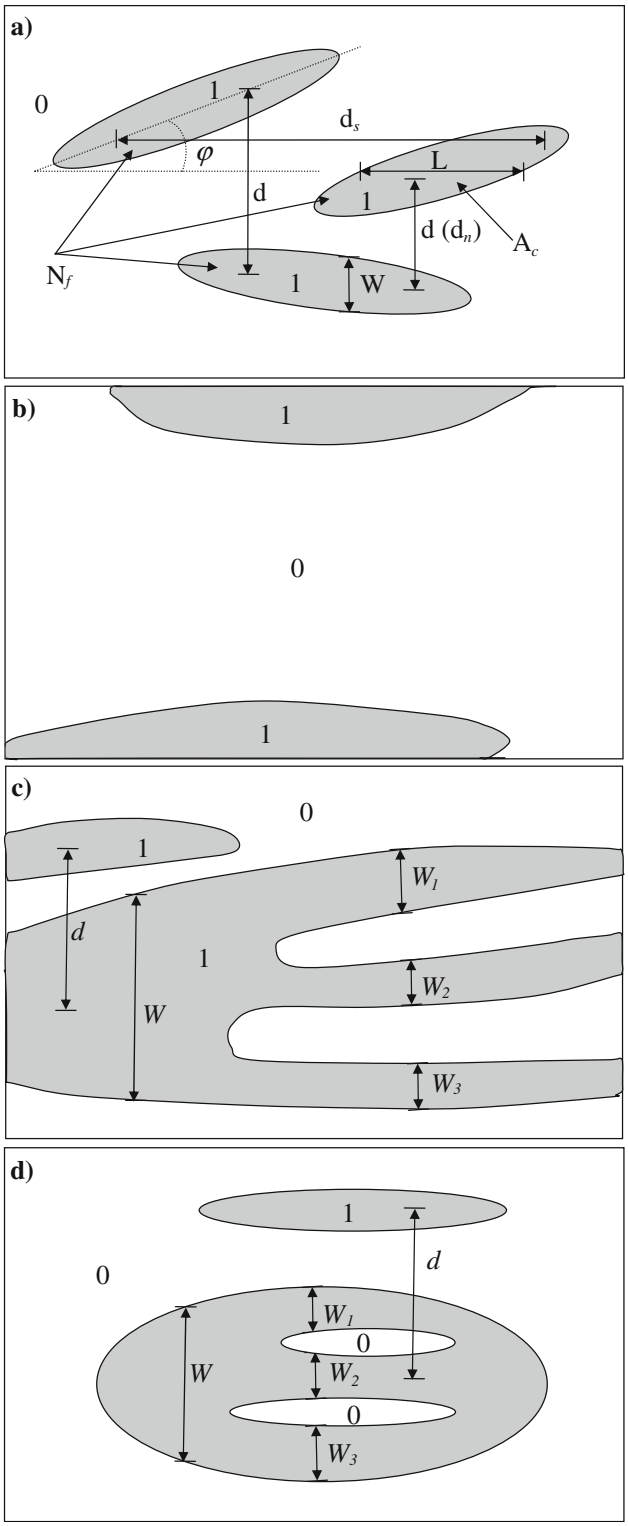

Fig. 3 Various conditions for statistical analysis

Ganapathisubramani et al. (2005) have found that low-speed streaks are statistically more significant than high-speed ones in the logarithm layer. Figure 4 shows that it is true even in the buffer layer.

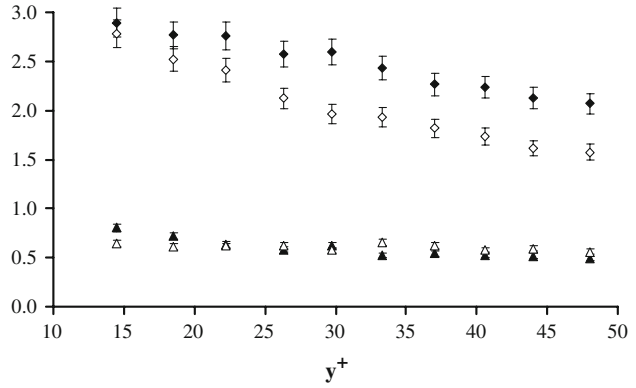

Fig. 4 Frequency of appearance of detected streaks N_f and bifurcated streaks N_b. N_f (LSS): *filled diamond*; N_f (HSS): *open diamond*; N_b (LSS): *filled triangle*; N_b (HSS): *open triangle*

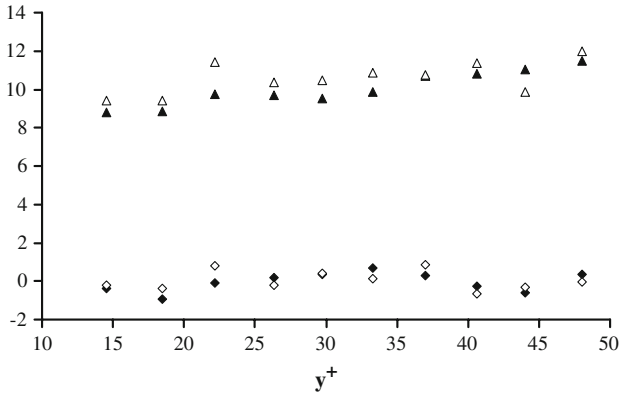

Fig. 5 Mean and RMS of the spanwise angle φ of streaks. $\bar{\varphi}$ (LSS): *filled diamond*; $\bar{\varphi}$ (HSS): *open diamond*; RMS (LSS): *filled triangle*; RMS (HSS): *open triangle*

Many streaks show a bifurcating behavior. Figure 4 also shows the frequency of appearance of bifurcated streaks (N_b) at various wall distances. This frequency is about 0.6 for both low- and high-speed streaks. For low-speed streaks, an increasing trend is observed when approaching the wall. Comparing with the value of N_f, it suggests that about 22–26% of low-speed streaks and about 23–35% of high-speed streaks have branches.

4.2 Spanwise angle

Streaks are generally expected to be parallel to the streamwise direction. Benefiting from the instantaneous character of the data, the angle of streaks with respect to the streamwise direction can be calculated. Because of the limitation in the size of SPIV images, streaks, which are cut by the spanwise border of the image, were excluded from the angle calculation. Figure 5 shows the variation of the mean spanwise angle $\bar{\varphi}$ and its RMS with wall distances. The values of $\bar{\varphi}$ are nearly zero for both low- and high-speed streaks, which suggests that on average streaks move parallel to the streamwise direction as expected. The near-zero value also confirms the homogeneous property of the flow in the spanwise direction. In Fig. 5, the RMS of φ is around 10° for both low- and high-speed streaks. Both types of streaks have a similar behavior: a slight increase with wall distance. Low- and high-speed streaks have nearly the same mean value of the RMS: about 7.2°. The small fluctuations in Fig. 5 result from the lack of convergence.

To investigate the spanwise angle in more detail, the histograms of φ for low- and high-speed streaks are shown, respectively, in Fig. 6 at selected wall distances. Different from the average behavior, Fig. 6 shows that many streaks move with a spanwise angle up to about 15°. Some of them even travel downstream with an angle of more than 25°. The high values of spanwise angle indicate the meandering property of streaks, which has been investigated by other researchers. Talmon et al. (1986) observed that the low-speed streaks detected from their flow visualization studies show time-dependent meanders in the spanwise direction, where they merge together or separate. Johansson et al. (1991) also found the meandering property of low-speed streaks from the results obtained from direct numerical simulation. Their results showed that the development of asymmetry in the spanwise direction is important for the

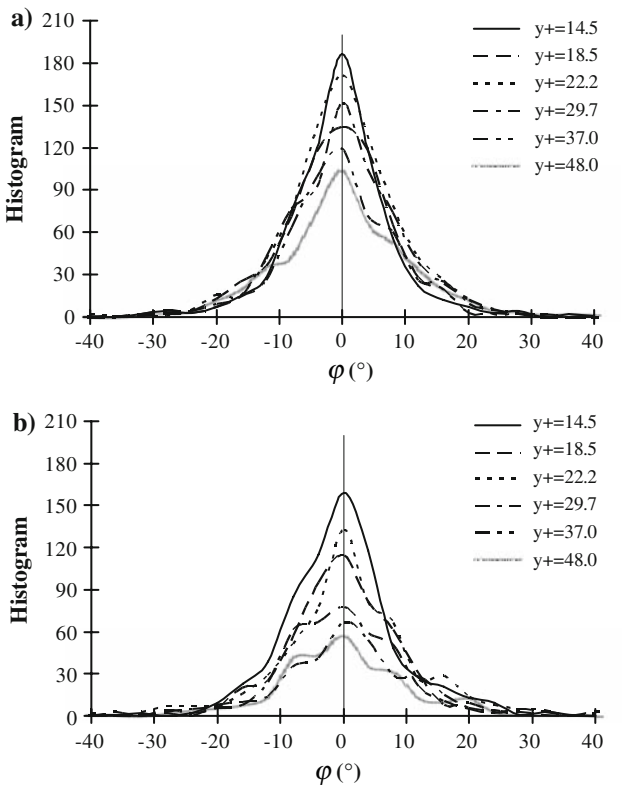

Fig. 6 Histogram of the spanwise angle φ of streaks at selected wall distance. **a** LSS; **b** HSS

evolution of near-wall structures. Based on that, they suggested that the inhibition of spanwise motion of the near-wall streaky pattern might be the primary reason for skin friction reduction. Landahl (1990) investigated the sublayer streaks by means of a simplified theoretical model. He found that asymmetry structures will grow in the streamwise direction and turn into streaks by the small three-dimensional disturbances initially localized in the spanwise direction, while symmetric structures showed little or no such behavior.

In Fig. 6, when the wall distance increases, a plateau begins to appear around 10–12°. This is consistent with the results of Ganapathisubramani et al. (2003). They found that the cores of a series of vortices and the zones of uniform momentum related to them are sometimes oriented at an angle of 10–20° to the streamwise direction in the streamwise–spanwise plane. Figure 6 also shows that this abovementioned plateau is more visible in the histogram of high-speed streaks than for the low-speed ones. This can partly be explained by the hairpin packet theory (Adrian et al. 2000; Tomkins and Adrian 2003; Ganapathisubramani et al. 2003; Hutchins et al. 2005). In this theory, low-speed streaks are inside of hairpin packets but high-speed streaks are outside of them. The hairpins in the packets can hold low-speed streaks between their legs at a similar streamwise orientation, preventing them from moving further in the spanwise direction. Since high-speed streaks are outside the packets, this influence is very limited.

The histograms in Fig. 6 are closer to a Laplace distribution than to a Gaussian one. The probability density function of a Laplace distribution is defined as

$$P(x) = \frac{1}{2b} e^{-|x-\mu|/b} \tag{7}$$

where μ is the mean and b is the parameter of rate of change.

To characterize the distribution of φ statistically, skewness (S) and flatness (F) are calculated and shown in Fig. 7. Skewness (S) is nearly zero for all wall distances, revealing the symmetry property of the distribution and confirming again the spanwise homogeneity. The value of flatness (F) is in the range of 5–7, which is comparable to 6, the standard value for a Laplace distribution. The variation of F near the wall should be attributed to the convergence.

4.3 Width

In Fig. 8, the mean width $\overline{W_a^+}$ of streaks is shown at various wall distances. The error bars represent an error of 5% of the mean. For low-speed streaks, the mean width $\overline{W_a^+}$ is nearly a constant at about 31 wall units in the region $14.5 < y^+ < 33$. After that, it increases slowly with the wall distance up to 39 wall units at $y^+ = 48$. This growing

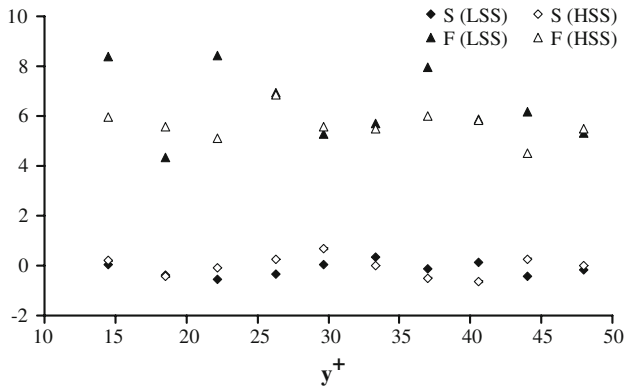

Fig. 7 Skewness (S) and flatness (F) of the spanwise angle φ of streaks

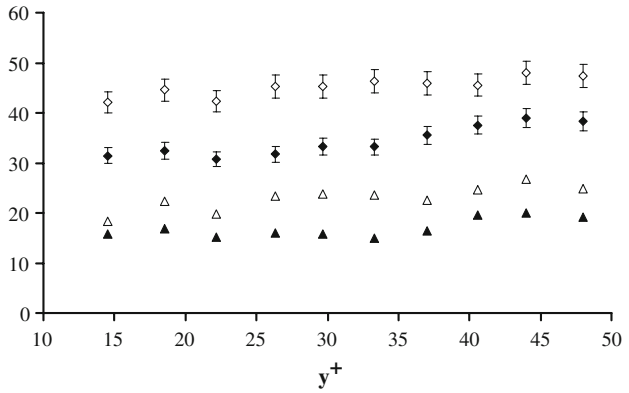

Fig. 8 Mean and RMS of the width $W^+{}_a$ of streaks. $\overline{W_a^+}$ (LSS): *filled diamond*; $\overline{W_a^+}$ (HSS): *open diamond*; RMS (LSS): *filled triangle*; RMS (HSS): *opend triangle*

tendency is in good agreement with the results of Tomkins and Adrian (2003). They found that the mean spanwise width of low-momentum regions increases almost linearly with wall distance in the logarithm layer, which is consistent with the attached-eddy hypothesis and self-similar growth of the structures. For high-speed streaks, the mean width $\overline{W_a^+}$ is fluctuating between 42 and 47 wall units. Carlier (2001), with a threshold $C_T = 1$, found that the width $\overline{W_a^+}$ is about 30 wall units for low-speed streaks and 50 wall units for high-speed streaks at $y^+ = 15$. These values are similar to the present results. Figure 8 also gives the RMS of the width $W^+{}_a$ of streaks. It shows that the RMS is about 16 wall units for low-speed streaks and 23 wall units for the high-speed ones in the whole y^+ range.

In the present study, the histograms of the width of streaks are also obtained and given in Fig. 9. These distributions are far from Gaussian, looking more like a lognormal distribution. Consequently, the most probable value is rather different from the mean value. For example, they are 20 and 30 wall units, respectively, for low-speed streaks at $y^+ = 14.5$. As shown in Fig. 9, the distribution

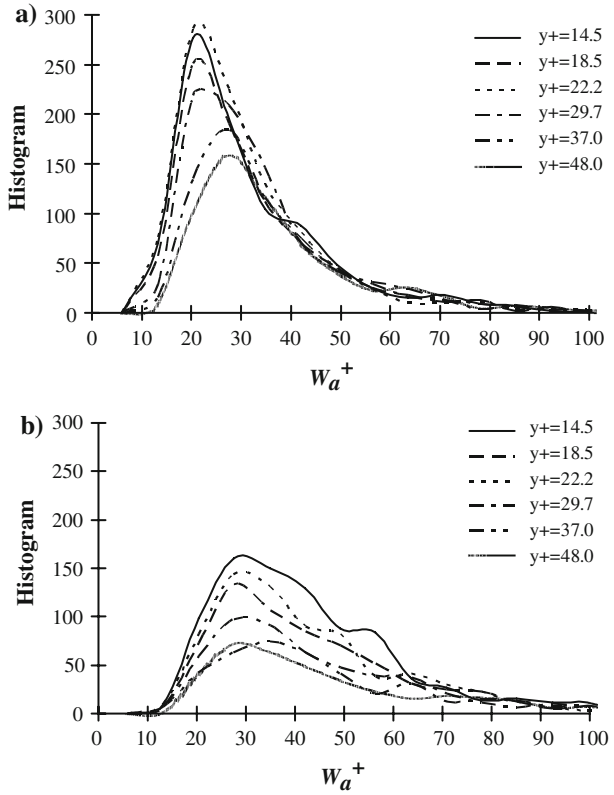

Fig. 9 Histogram of the width W_a^+ of streaks at selected wall distances. **a** LSS; **b** HSS

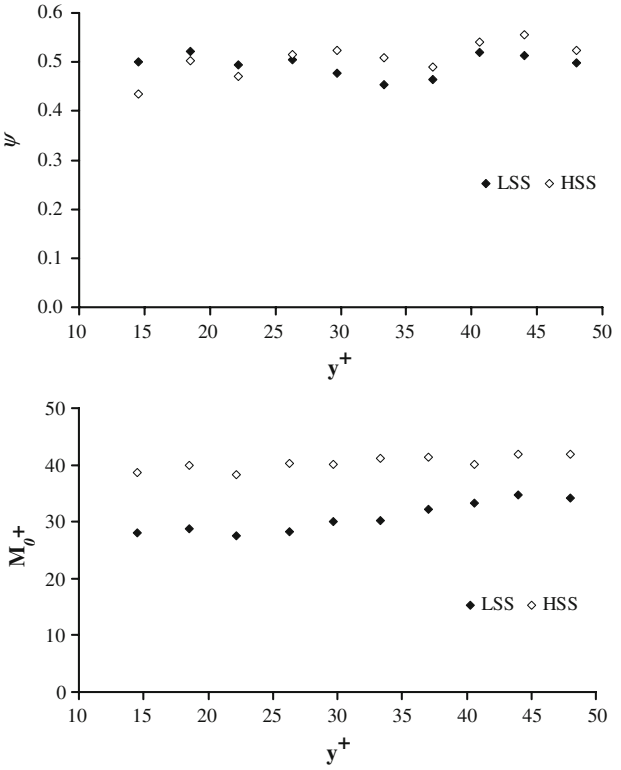

Fig. 10 Variation coefficient ψ and median value M^+_0 of the width W^+_a of streaks

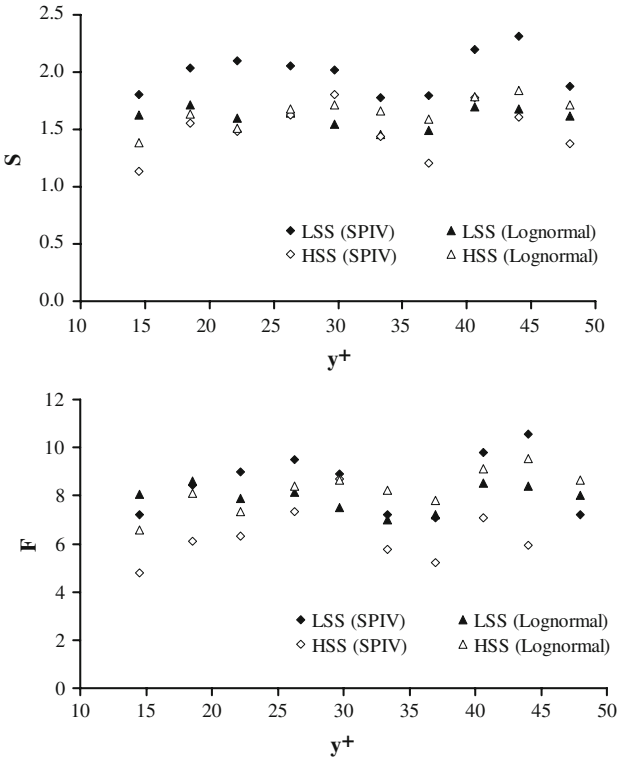

Fig. 11 Comparison of skewness (S) and flatness (F) of the width W_a^+ of streaks of the present study with the theoretical values obtained according to lognormal distributions

of high-speed streaks is significantly wider than the low-speed ones. The most probable value is between 20 and 30 wall units for low-speed streaks and between 25 and 35 wall units for high-speed ones. It is interesting to compare the characteristics of the present distribution to a true lognormal one.

According to Hastings and Peacock (1975), let us consider that the variable A has a lognormal distribution, and $\bar{A}$ and σ_A are the corresponding mean value and standard deviation, respectively. The variation coefficient ψ is defined by

$$\psi = \frac{\bar{A}}{\sigma_A} \tag{8}$$

The probability density function is given by

$$P(A) = \frac{e^{-\frac{1}{2}\left(\frac{1}{\psi_0}\ln\frac{A}{M_0}\right)^2}}{A\psi_0\sqrt{2\pi}} \tag{9}$$

where

$$M_0 = \bar{A}(1+\psi^2)^{-\frac{1}{2}} \tag{10}$$

$$\psi_0 = (\ln(1+\psi^2))^{\frac{1}{2}} \tag{11}$$

Here, M_0^+ is the median value of A and ψ_0 the variation coefficient of ln ψ. Employing Eqs. 8, 10, and 11, the

coefficient ψ and the median value M_0^+ of the width W_a^+ of streaks are calculated and shown in Fig. 10. The range of ψ of all 10 distribution is $0.45 < \psi < 0.52$ and $0.43 < \psi < 0.56$ for low- and high-speed streaks, respectively. The difference in the range of ψ can be explained by the fact that the distribution of W_a^+ for high-speed streaks is wider than that for low-speed ones, as shown clearly by Fig. 9. ψ_0 is about 4–6% smaller than ψ for both types of streaks at all wall distance studied. Compared with Fig. 8, the value of M_0^+ in Fig. 10 has nearly the same distribution as $\overline{W_a^+}$, except that it is about 9–12% smaller.

According to Eq. 9, the theoretical skewness and flatness of the lognormal distribution are defined by

$$S = \left(e^{\psi_0^2} + 2\right)\sqrt{e^{\psi_0^2} - 1} \tag{12}$$

$$F = e^{4\psi_0^2} + 2e^{3\psi_0^2} + 3e^{2\psi_0^2} - 3 \tag{13}$$

Using Eqs. 12 and 13, the theoretical skewness (S) and flatness (F) of lognormal distributions corresponding to ψ_0 and M_0^+ in Fig. 10 are obtained and compared with the present results in Fig. 11. For both S and F, the present results are comparable with theoretical ones. In general, for S, the agreement is better for high-speed streaks than for low-speed ones. However, for F, the opposite is true. This result indicates that the distribution of W_a^+ is more symmetric for high-speed streaks than that for low-speed ones, as shown in Fig. 9. According to Hastings and Peacock (1975), for a true lognormal distribution, the ratio of the most-probable value to the mean value R_{mm}, can be calculated by Eq. 14. Figure 12 shows that the present results are consistent with the theoretical values. It reveals again that the width of streaks follows nearly a lognormal distribution.

$$R_{\mathrm{mm}} = (1 + \psi^2)^{-\frac{3}{2}} \tag{14}$$

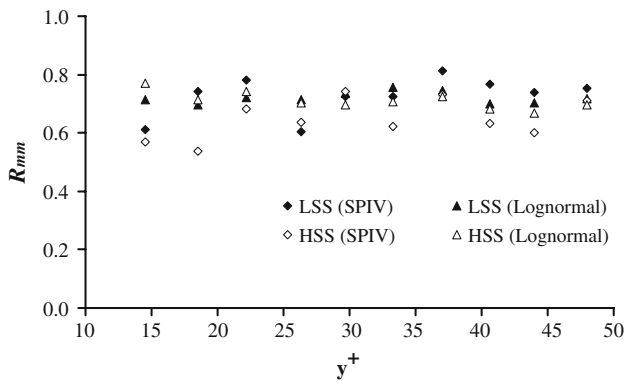

Fig. 12 Ratio of the most probable value to the mean value R_{mm} of the width W_a^+ of streaks

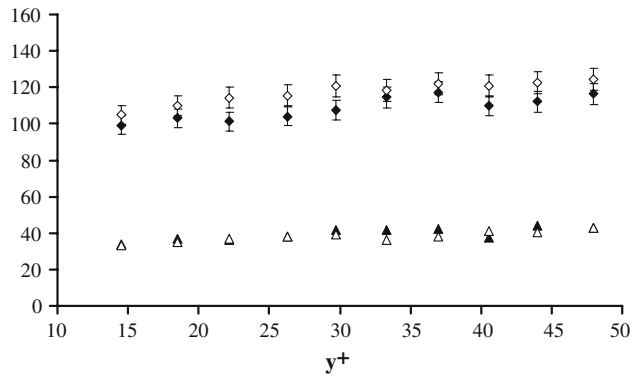

Fig. 13 Mean and RMS of the spanwise distance between the nearby streaks d^+. $\overline{d^+}$ (LSS): *filled diamond*; $\overline{d^+}$ (HSS): *open diamond*; RMS (LSS): *filled triangle*; RMS (HSS): *open triangle*

4.4 Spanwise distance

The mean spanwise distance $\overline{d^+}$ between the center of two nearby streaks is widely referred to as the spanwise periodic spacing $\bar{\lambda}$ in literature. Figure 13 shows $\overline{d^+}$ for low- and high-speed streaks at various wall distances. The error bars represent an error of 5% of the mean. The mean distance $\overline{d^+}$ is nearly the same for both types of streaks at the same wall distance. It varies between 114 and 135 wall units. Figure 13 also suggests that the mean distance $\overline{d^+}$ is slightly smaller in the lower part of the buffer layer ($y^< = 30$) than that in the upper part of the buffer layer ($y^> = 30$). Figure 13 also gives the RMS of d^+. The value of this RMS is about 42 wall units for low-speed streaks and 39 wall units for high-speed streaks.

The mean distance $\overline{d^+}$ between low-speed streaks are compared with earlier studies in Fig. 14. Smith and Metzler (1983) obtained their results at $Re_\theta = 2{,}030$, using a high-speed video camera and a hydrogen bubble-wire in water. In spite of the differences in the experimental methods and conditions, the present results are comparable with their results, except at $y^+ = 30$, where Smith and Metzler (1983) observed a much larger value (see Fig. 14).

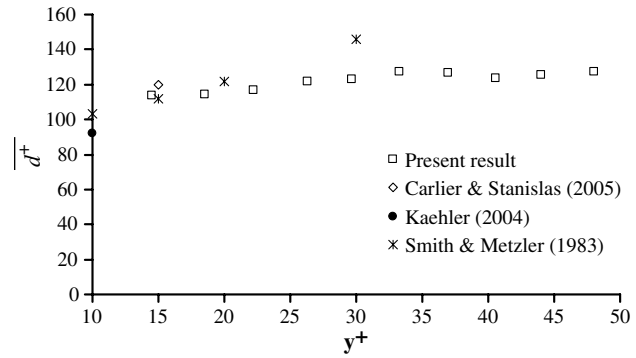

Fig. 14 Comparison of the mean spanwise distance $\overline{d^+}$ of low-speed streaks

Schraub and Kline (1965) were the first to examine the variation of streak spacing with wall distance by using both visual inspection and spectral methods. They found that streak spacing appears to increase for $y^+ \geq 7$; however, no explanation was provided for this increase. Nakagawa and Nezu (1981), using both visual techniques and hot film probe correlation techniques, showed an apparent increase in streak spacing for $y^+ > 10$ and proposed an estimation of this spacing as $2y^+$ when $y^+ > 100$. They suggested that the increase in scale may be due to a pairing interaction of the low-speed streaks as they move outward from the wall, resulting in the increase in scale. Figure 14 shows that both the present study and the results of Smith and Metzler (1983) indicate an increase of $\overline{d^+}$ with wall distance, which agrees well with the above-mentioned studies. It should be noted that the increase of $\overline{d^+}$ is much stronger in the study by Smith and Metzler (1983) than that in the present study. Kaehler (2004) has also conducted an analysis on $\overline{d^+}$ using the spatial correlation method. Figure 14 shows that the result of Kaehler (2004) is smaller than the other results. The difference can be explained by the fact that it is obtained directly from the spatial correlation of negative streamwise velocity fluctuations. In this correlation, the regions with very small streamwise velocity fluctuations are also considered as parts of low-speed streaks. Moreover, the correlation technique cannot remove the regions that have large values of $-u'$ but are too small to be considered as parts of low-speed streaks. Carlier and Stanislas (2005) used standard 2D2C PIV on a larger field of view ($1{,}250^+ \times 800^+$), at the same Reynolds number as here, to investigate streaks at $y^+ = 15$. Their results are in good agreement with the present study.

The instantaneous indicative images of streaks allow to obtain the histogram of the distance d^+. In Fig. 15, the number of samples decrease sharply with wall distance. This can be explained by the following two reasons. One is that the number of streaks decreases with the wall distance as shown in Fig. 4. The other is that streaks become wider with the wall distance (see Fig. 8). The wider streaks are, the more likely they will be cut by the spanwise border of the field and thus the number of samples will decrease. Moreover, the streamwise extension of streaks may decrease with wall distance, as velocity fluctuations decrease. The shorter streaks are, the fewer samples there are. Unfortunately, due to the relatively small size of the SPIV field used, it is not possible to measure the length of streaks.

Except for oscillations that may arise from the lack of convergence, both histograms of low- and high-speed streaks are close to a Rayleigh distribution (Weisstein 1999). The probability distribution function of this distribution is defined as

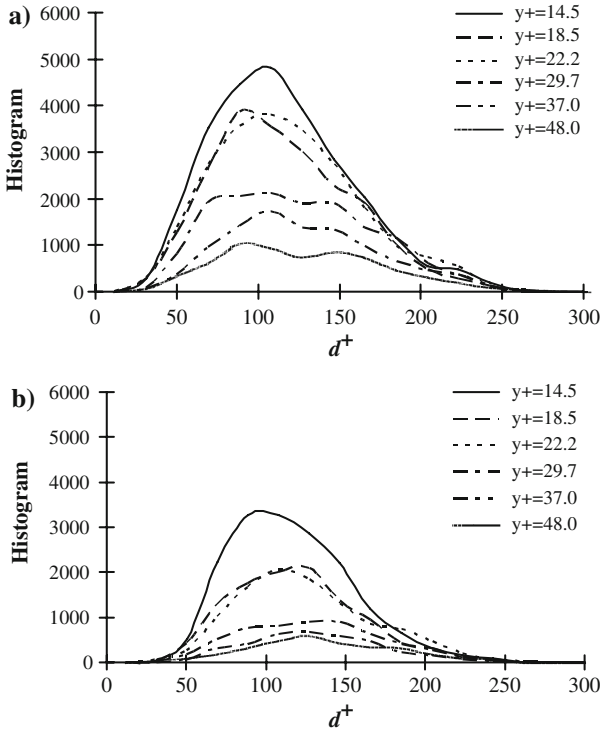

Fig. 15 Histogram of the spanwise distance between the nearby streaks d^+ at selected wall distance. **a** LSS; **b** HSS

$$P(x) = \frac{(x-a)e^{-(x-a)^2}/2s^2}{s^2} \tag{15}$$

where a is the shift to the origin, s is the rate of change parameter, and $x \in [a, \infty]$.

To characterize the histogram from the statistical point of view, skewness (S) and flatness (F) are calculated and are given in Fig. 16. These parameters are compared with those obtained from a Rayleigh distribution. For such a distribution, skewness (S) and flatness (F) are defined by Eqs. 16 and 17. For both low- and high-speed streaks, the values of the two parameters are nearly the same. Skewness (S) has a value about 0.4 and flatness (F) has a value of about 2.8. These values are comparable, respectively, to $S = 0.63$ and $F = 3$, the standard values for a Rayleigh distribution.

$$S = \frac{2(\pi-3)\sqrt{\pi}}{(4-\pi)^{3/2}} \tag{16}$$

$$F = \frac{6\pi^2 - 24\pi + 16}{(4-\pi)^2} + 3 \tag{17}$$

According to Nakagawa and Nezu (1981) and Smith and Metzler (1983), the distance between nearby low-speed streaks d^+ follows a lognormal distribution. To compare with their results, the variation coefficient ψ, skewness (S), and flatness (F) are presented. Figure 17 compares ψ

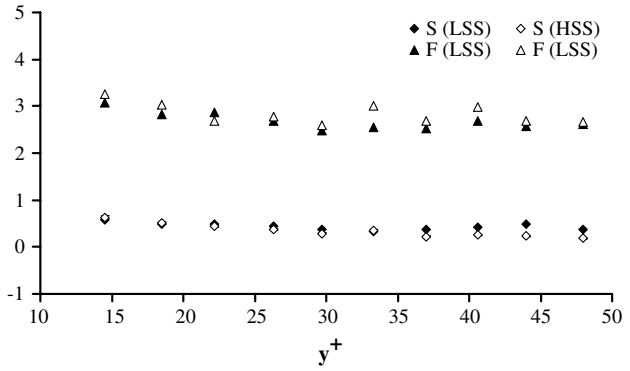

Fig. 16 Skewness (S) and flatness (F) of the spanwise distance d^+ between the nearby streaks

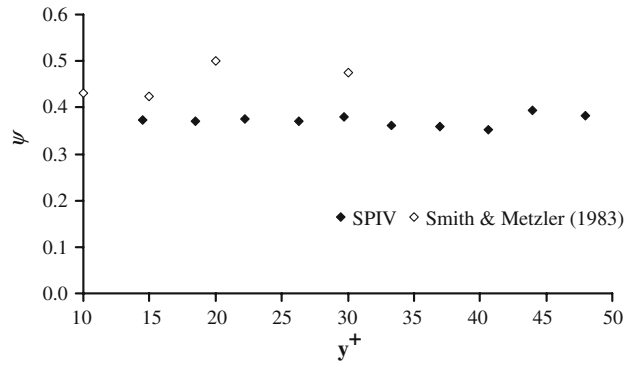

Fig. 17 Comparison of variation coefficient ψ of the spanwise distance d^+ of low-speed streaks obtained in the present study with the results of Smith and Metzler (1983)

obtained from the present results with those found by Smith and Metzler (1983). It shows that the present results are smaller than those of Smith and Metzler (1983) but still comparable. Figure 18 gives skewness (S) and flatness (F) of d^+ obtained from the experiments compared with the theoretical values computed from ψ_0 (Eqs. 11–13). The experimental results turn out to be very similar. For both skewness (S) and flatness (F), the theoretical values are about two times higher than those obtained by experiments. This suggests that the distribution of d^+ does not follow a lognormal distribution. As proposed above, d^+ is near to a Rayleigh distribution (see Fig. 15). This proposition is supported by the values of skewness and flatness in Fig. 18.

Most of the former studies were conducted to measure only the spanwise distance between two nearby streaks d^+. In the present study, however, instantaneous streak-indicative images provide the possibility to measure the spanwise distance between the center of two closest streaks and its mean value (referred to as d_n^+ and $\overline{d_n^+}$, respectively, in Fig. 3a). Figure 19 shows the mean distance $\overline{d_n^+}$ at various wall distances. Comparing with Fig. 13, the distance $\overline{d_n^+}$ is about 13 wall units smaller than $\overline{d^+}$ for low-speed

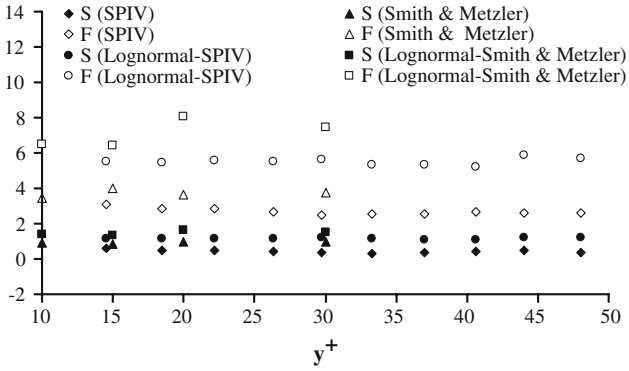

Fig. 18 Comparison of skewness (S) and flatness (F) of the spanwise distance d^+ of low-speed streaks obtained in the present study with the results of Smith and Metzler (1983), and theoretical values from lognormal distributions

streaks and about 9 wall units for high-speed streaks. This difference indicates a staggering of the two closest streaks in the streamwise direction (Fig. 3a). Except for the difference in value, $\overline{d^+}$ and $\overline{d_n^+}$ have a similar distribution with wall distance, which manifests the reliability of the measurement. Figure 19 also shows that the RMS of d_n^+ is around 39 wall units for both low- and high-speed streaks on average. The present study has also examined the histograms of the spanwise distance d_n^+ for both low- and high-speed streaks. The result shows that, same as d^+, d_n^+ has a nearly Rayleigh distribution. It also reveals that about 60–70% of d^+ are d_n^+.

In the present study, the threshold procedure is the first step to detect streaks from the velocity fields and thus has a direct influence on the statistical results. To evaluate this influence, several different threshold values (C_T) ranging from 0.5 to 1.0 have been tested at $y^+ = 14.5$. Taking the results from $C_T = 0.6$ as a reference, the comparison shows that the threshold value has some influence on the mean values. For the width and the frequency of appearance, the maximum difference is about 10 and 4.5%,

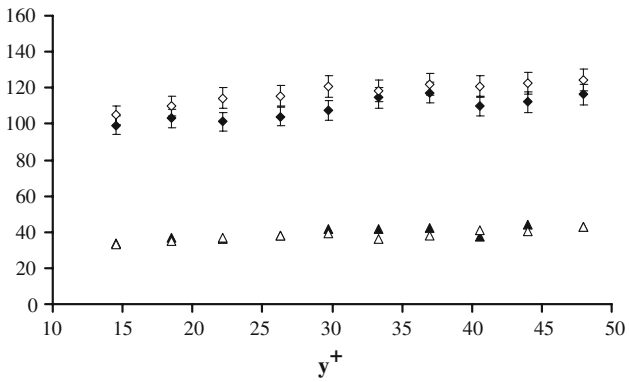

Fig. 19 Mean and RMS of the spanwise distance between the closest streaks d_n^+. $\overline{d_n^+}$ (LSS): *filled diamond*; $\overline{d_n^+}$ (HSS): *open diamond*; RMS (LSS): *filled triangle*; RMS (HSS): *open triangle*

respectively, in the range of thresholds tested. This difference is less than 2.5% for all the other characteristics. Moreover, the threshold value has nearly no influence on the profiles of the variation with wall distance for the statistics of all the characteristics studied in the present study. The influences of the structuring element (M_S) and the clean factors (C_B and C_C) on statistics have also been studied. The results show that they have a smaller influence when compared to the threshold value.

As discussed earlier, the histogram of each characteristic has been assumed to be similar with one theoretical distribution. However, it is not easy to compare all the curves with their corresponding theoretical distributions due to the following two reasons. Firstly, each characteristic has been obtained at 10 different wall distances and thus have 10 different histograms for both low- and high-speed streaks. Secondly, at each wall distance, the theoretical distribution needs to be adjusted according to corresponding parameters obtained from SPIV. Therefore, only the histogram of low-speed streaks at $y^+ = 14.5$ is selected to exemplify the comparison of results from SPIV with the corresponding theoretical distributions. To simplify the comparison, the histograms obtained from SPIV are converted into PDFs. The results of the comparison are shown in Fig. 20. The theoretical PDFs are built based on the Eqs. 7, 9, and 15 with the corresponding parameters obtained from SPIV. This figure reveals clearly that the results from SPIV are in very good agreement with the corresponding theoretical ones.

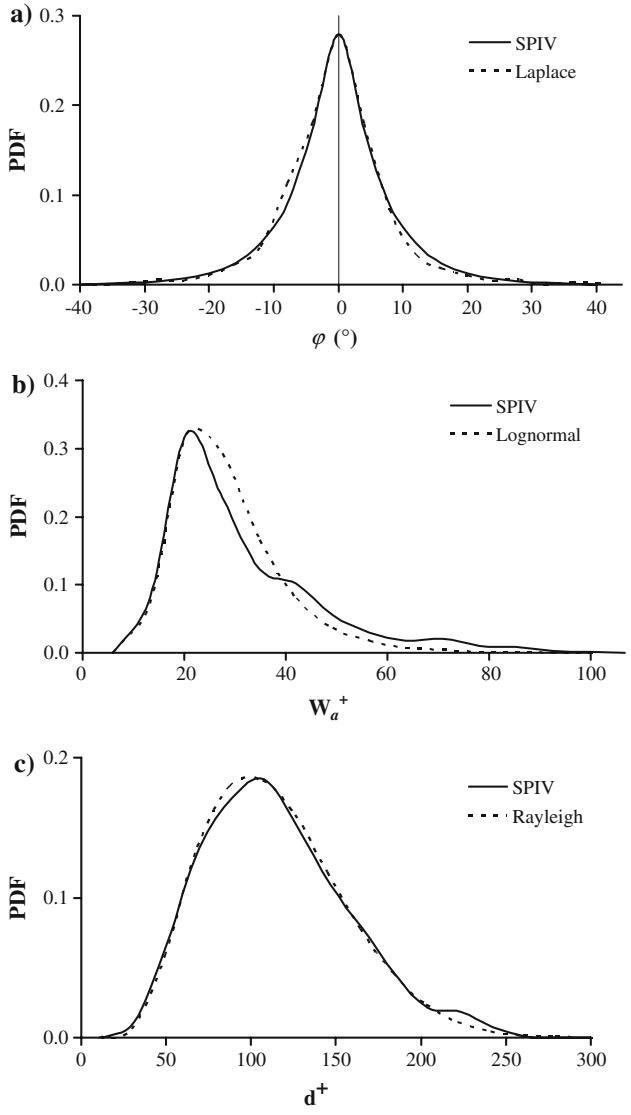

Fig. 20 Comparison of the PDFs of different characteristics obtained from SPIV with corresponding theoretical results at $y^+ = 14.5$. **a** φ, **b** W_a^+, **c** d^+

4.5 Percentage of area

Table 2 shows the percentage of the total area of low- and high-speed streaks in the whole field with various wall distance. With the selected detection parameters, low- and high-speed streaks cover about 59% of the area of the whole field at $y^+ = 14.5$. This percentage decreases nearly linearly to about 45% at $y^+ = 48$ with wall distance. Table 2 shows that the percentage of total area of high-speed streaks is almost equal to that of the low-speed ones.

Table 3 shows a comparison of the percentages in the present study with those of Carlier (2001). It shows that the present percentage is greater. This difference is attributed to the threshold of 0.6–0.75 (from wall distance $y^+ = 14.5$ to $y^+ = 48$), while Carlier (2001) used a constant value of 1.0. With the same threshold, the results become more similar, which indicates that the choice of the threshold is important in this type of study.

4.6 Mean normalized velocity fluctuations

Figure 21 gives the mean normalized velocity fluctuations in streaks at various wall distances. The mean streamwise normalized fluctuations in low-speed streaks are comparable to those in high-speed ones. In low-speed streaks, remarkably, high positive mean wall-normal fluctuations are observed. Similarly, high negative mean wall-normal fluctuations are found in high-speed streaks. These findings confirm that ejections are associated with low-speed streaks, while sweeps are linked to high-speed ones (Adrian et al. 2000; Ganapathisubramani et al. 2003, 2005). Very close to the wall ($y^+ < 18.5$), the absolute value of the mean wall-normal fluctuation is comparable in both low- and high-speed streaks. In the region $y^+ > 18.5$, it is slightly larger in low-speed streaks than that in high-speed ones. The nearly zero value of the mean spanwise fluctuation in both low- and high-speed streaks results from the spanwise homogeneity.

Table 2 Percentage of the total area of low- and high-speed streaks with various wall distance

	y^+									
	14.5	18.5	22.2	26.3	29.7	33.3	37.0	40.6	44.0	48.0
Total area of LSS/area of whole field	0.29	0.28	0.26	0.25	0.25	0.23	0.23	0.23	0.22	0.22
Total area of HSS/area of whole field	0.30	0.29	0.27	0.27	0.26	0.26	0.24	0.24	0.23	0.23

Table 3 Percentage of the total area of low- and high-speed streaks, comparison with the results of Carlier (2001)

	Present results						Carlier's results		
y^+	14.5	14.5	26.3	26.3	48.0	48.0	15.0	25.0	50.0
Threshold C_T	0.60	1.00	0.65	1.00	0.75	1.00	1.00	1.00	1.00
Total area of LSS/total area of LSS and HSS	0.50	0.51	0.48	0.50	0.49	0.50	0.48	0.52	0.52
Total area of LSS and HSS/area of whole field	0.59	0.34	0.52	0.31	0.45	0.31	0.31	0.29	0.31

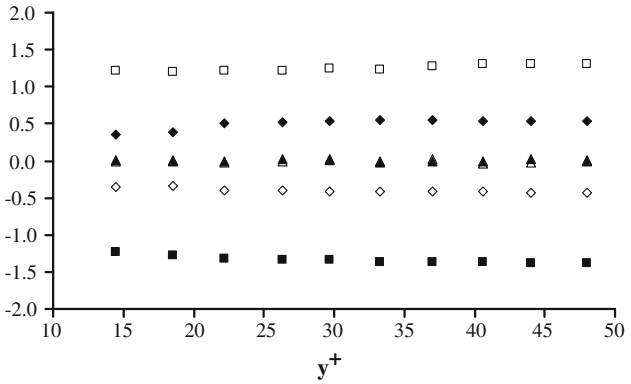

Fig. 21 Mean normalized velocity fluctuations in streaks. $\frac{u'}{\sigma_u}$ (LSS): *filed square*; $\frac{v'}{\sigma_v}$ (LSS): *filled diamond*;$\frac{w'}{\sigma_w}$ (LSS): *filled triangle*; $\frac{u'}{\sigma_u}$ (HSS): *open square*; $\frac{v'}{\sigma_v}$ (HSS): *open diamond*; $\frac{w'}{\sigma_w}$ (HSS): *open triangle*

5 Conclusions

Applying a pattern recognition method on the instantaneous 2D3C velocity fields obtained from SPIV dataset, both low- and high-speed streaks were identified and the corresponding binary images were created. From these images, the statistical characteristics of streaks were investigated in detail in the region $14.5 < y^+ < 48$. The results are generally in good agreement with previous studies. More importantly, this study investigates additional statistical characteristics of streaks and expands greatly the information about them.

In the lower part of the buffer ($y^+ \leq 30$), with an increasing wall distance, the frequency of appearance decreases relatively rapidly for high-speed streaks, but is nearly the same or decreases very slowly for low-speed ones. In the upper part of the buffer ($y^+ > 30$), with increasing wall distance, the frequency of both low- and high-speed streaks decreases nearly linearly and with similar declining rate. On average, about 2.9 low-speed streaks and 2.8 high-speed ones are expected per area of $530^+ \times 300^+$ at $y^+ = 14.5$, while about 2.1 low-speed streaks and 1.6 high-speed ones at $y^+ = 48$. In general, about 22–26% of low-speed streaks and about 23–35% of high-speed streaks show a bifurcating behavior.

The mean spanwise angle of both low- and high-speed streaks is nearly zero, indicating the homogeneous property in the spanwise direction. The histogram of the spanwise angle follows nearly a Laplace distribution. It shows that many streaks have a spanwise angle larger than 15°, evidencing the meandering behavior of these structures.

The mean width of low-speed streaks is nearly constant at about 31 wall units in the region $14.5 < y^+ < 33$. Above that region, it increases slowly with the wall distance up to 39 wall units. For high-speed streaks, the mean width varies between 42 and 47 wall units in the whole range studied. Clearly, high-speed streaks are wider than low-speed ones. For both types of structures, the histogram of the width is close to a lognormal distribution.

The mean spanwise distance between the center of two nearby low-speed streaks is nearly the same as that of high-speed ones. It varies between 114 and 135 wall units. The present results suggest that this distance is slightly smaller in the lower part of the buffer layer ($y^+ < 30$) than that in the upper part of the buffer ($y^+ > 30$). In the present study, it is the first time that the spanwise distance between the center of two closest low- (or high-) speed streaks and its mean value were investigated. In comparison with the mean spanwise distance between the centers of two nearby streaks, this distance is smaller for both low- and high-speed streaks. This difference indicates a staggering of two closest streaks in the streamwise direction. Except for the difference in value, the two distances (between two nearby streaks and between two closest streaks) have a similar distribution with wall distance. The histogram of spanwise distance of two nearby streaks or two closest ones follows nearly a Rayleigh distribution.

The total area of low-speed streaks is almost equal to that of high-speed ones. Both the areas decrease nearly linearly with wall distance. The present study shows that the magnitude of these fluctuations is nearly the same in both types of the structures. In low-speed streaks, high positive wall-normal fluctuations are observed together with high negative streamwise ones. The contrary is true in high-speed streaks.

References

Achia BU, Thompson DW (1977) Structure of the turbulent boundary in drag-reducing pipe flow. J Fluid Mech 81:439–464

Adrian RJ (1991) Particle imaging techniques for experimental fluid mechanics. Annu Rev Fluid Mech 23:261–304

Adrian RJ, Meinhart CD, Tomkins CD (2000) Vortex organization in the outer region of the turbulent boundary layer. J Fluid Mech 422:1–54

Bippes H (1972) Experimentelle untersuchung des laminar-turbulenten umschlags an einer parallel angestroemten konkaven wand. Heidelb Akad Wiss, Math Naturwiss Kl, pp 103–180

Blackwelder RF, Eckelmann H (1979) streamwise vortices associated with the bursting phenomenon. J Fluid Mech 94:577–594

Carlier J (2001) Etude des structures cohérentes de la turbulence de paroi á grand nombre de reynolds par vélocimétrie par images de particules. PhD Thesis, Univercity Lille 1

Carlier J, Stanislas M (2005) Experimental study of eddy structures in a turbulent boundary layer using paritcle image velocimetry. J Fluid Mech 535:143–188

Coudert S, Schon JP (2001) Back projection algorithm with misalignment corrections for 2D3C stereoscopic PIV. Meas Sci Technol 12:1371–1381

Ganapathisubramani B, Longmire EK, Marusic I (2003) Characteristics of vortex packets in turbulent boundary layers. J Fluid Mech 478:35–46

Ganapathisubramani B, Hutchins N, Hambleton WT, Longmire EK, Marusic I (2005) Investigation of large-scale coherence in a turbulent boundary layer using two-point correlations. J Fluid Mech 524:57–80

Gupta AK, Laufer J, Kaplan RE (1971) Spatial structure in the viscous sublayer. J Fluid Mech 50:493–512

Hama FR (1954) Boundry layer characteristics for smooth and rough surfaces. Trans Soc Nav Arch Mar Eng 62:233–255

Hastings NAJ, Peacock JB (1975) Statistical distribution: a handbook for students and practitioners. Wiley, New York

Hutchins N, Hambleton WT, Marusic I (2005) Inclined cross-stream stereo particle image velocimetry measurements in turbulent boundary layers. J Fluid Mech 541:21–54

Johansson AV, Alfredsson PH, Kim J (1991) Evolution and dynamics of shear-layer structures in near-wall turbulence. J Fluid Mech 224:579–599

Kaehler CJ (2004) Investigation of the spatio-temporal flow structure in the buffer region of a turbulent boundary layer by means of multiplane stereo PIV. Exp Fluids 36:114–130

Kline SJ (1978) The role of visualization in the study of the turbulent boundary layer. In: Smith CS, Abbott DE (eds) Workshop on coherent structure of turbulent boundary layers, Lehigh University, Bethlehem, PA, pp 1–26

Kline SJ, Reynolds WC, Schraub FA, Runstadler PW (1967) The structure of turbulent boundary layers. J Aeronaut Sci 30:741–773

Kreplin HP, Eckelmann H (1979) Propagation of pertubations in the viscous sublayer and adjacent wall region. J Fluid Mech 59:305–322

Lagraa B, Labraga L, Mazouz A (2004) Characterization of low speed streaks in the near-wall region of a turbulent boundary layer. Eur J Mech B Fluids 23:587–599

Landahl MT (1990) On sublayer streaks. J Fluid Mech 212:593–614

Lee MJ, Eckelman L, Hanratty TJ (1974) Identification of turbulent wall eddies through the phase relation of the components of the fluctuating velocity gradient. J Fluid Mech 66:17–33

Lin J (2006) Etude détaillée des structures cohérentes de la zone tampon de la turbulence de paroi á l'aide de données de PIV stéréoscopique. PhD Thesis, Ecole centrale de Lille

Lin J, Laval JP, Foucaut JM, Pérenne N, Stanislas M (2008) Assessment of different SPIV processing methods for an application to near-wall turbulence. In: Schröder A, Willert CE (eds) Particle image velocimetry: new developments and recent applications. Topics in applied physics, vol 112. Springer, Berlin, pp 191–221

Matheron G (1975) Random sets and integral geometry. Wiley, New York

Nakagawa H, Nezu I (1981) Structure of space time correlations of bursting phenomena in an open channel flow. J Aeronaut Sci 104:1–43

Oldaker oK, Tiederman WJ (1977) Spatial structure of the viscous sublayer in drag-reducing channel flow. Phys Fluid 20:S133–S144

Pérenne N, Foucaut JM, Savatier J (2004) Study of the accuracy of different stereoscopic reconstruction algorithms. In: Stanislas M, Westerweel J, Kompenhans J (eds) Proceedings of the EUROPIV 2 workshop on particle image velocimetry, Zaragoza, Spain, March 31–April 1, 2003. Springer, Berlin, pp 375–390

Prasad AK, Adrian RJ (1993) Stereoscopic particle image velocimetry applied to liquid flows. Exp Fluids 15:49–60

Robinson SK (1991) Coherent motions in the turbulent boundary layer. Annu Rev J Fluid Mech 23:601–639

Runstadler PC, Kline SJ, Reynolds WC (1963) Department of Mechanical Engineering, MD-8, Stanford University Report

Schraub FA, Kline SJ (1965) A study of the structure of the turbulent boundary layer with and without longitudinal pressure gradients. Thermosciences Division, MD-12, Stanford University Report

Smith CR, Metzler SP (1983) The characteristics of low speed streaks in the near wall region of a turbulent boundary layer. J Aeronaut Sci 129:27–54

Soloff S, Adrian R, Liu Z (1997) Distortion compensation for generalized stereoscopic particle image velocimetry. Meas Sci Technol 8:1441–1454

Suzuki Y, Kasagi N (1993) Drag reduction mechanism on micro-grooved riblet surface. In: International conference on near-wall turbulent flows, Tempe, Arizona, 15–17 March 1993

Talmon AM, Kunen JMG, Ooms G (1986) Simultaneous flow visualization and Reynolds-stress measurement in a turbulent boundary layer. J Fluid Mech 163:459–478

Tomkins CD, Adrian RJ (2003) Spanwise structure and scale growth in turbulent boundary layers. J Fluid Mech 490:37–74

Weisstein EW (1999) Normal distribution. MathWorld—a Wolfram web resource

Westerweel J, van Oord J (1999) Stereoscopic PIV measurements in a turbulent boundary layer. In: Stanislas M et al (eds) EUROPIV: progress towards industrial application. Kluwer, Dordrecht, pp 459–478

Willert C (1997) Stereoscopic digital particle image velocimetry for applications in wind tunnel flows. Meas Sci Technol 8:1465–1479